Flow Boiling Enhancement in Microtubes With Crosslinked pHEMA Coatings and the Effect of Coating Thickness

Taha Çıkım
Mechatronics Engineering Program,
Faculty of Engineering Science,
Orhanli – Tuzla/Istanbul 34956, Turkey
e-mail: tahacikim@sabanciuniv.edu

Efe Armağan
Material Science and Engineering Program,
Faculty of Engineering Science,
Orhanli – Tuzla/Istanbul 34956, Turkey
e-mail: efearmagan@sabanciuniv.edu

Gozde Ozaydin Ince
Material Science and Engineering Program,
Faculty of Engineering Science,
Orhanli – Tuzla/Istanbul 34956, Turkey
e-mail: gozdeince@sabanciuniv.edu

Ali Koşar[1]
Mechatronics Engineering Program,
Faculty of Engineering Science,
Orhanli – Tuzla/Istanbul 34956, Turkey
e-mail: kosara@sabanciuniv.edu

In this experimental study, flow boiling in mini/microtubes was investigated with surface enhancements provided by crosslinked polyhydroxyethylmethacrylate (pHEMA) coatings, which were used as a crosslinker coating type with different thicknesses (∼50 nm, 100 nm, and 150 nm) on inner microtube walls. Flow boiling heat transfer experiments were conducted on microtubes (with inner diameters of 249 μm, 507 μm, and 908 μm) coated with crosslinked pHEMA coatings. pHEMA nanofilms were deposited with initiated chemical vapor deposition (iCVD) technique. De-ionized water was utilized as the working fluid in this study. Experimental results obtained from coated microtubes were compared to their plain surface counterparts at two different mass fluxes (5000 kg/m^2 s and 20,000 kg/m^2 s), and significant enhancements in critical heat flux (up to 29.7%) and boiling heat transfer (up to 126.2%) were attained. The enhancement of boiling heat transfer was attributed to the increase in nucleation site density and incidence of bubbles departing from surface due to porous structure of crosslinked pHEMA coatings. The underlying mechanism was explained with suction-evaporation mode. Moreover, thicker pHEMA coatings resulted in larger enhancements in both CHF and boiling heat transfer.
[DOI: 10.1115/1.4027352]

Keywords: crosslinked pHEMA coating, heat transfer enhancement, flow boiling, microscale boiling

Introduction

A wide spectrum of microscale flow boiling applications encourages researchers to study boiling heat transfer mechanisms in microscale. As a result, many studies related to microscale boiling heat transfer are now available in the literature [1–12]. One of the most significant issues in boiling heat transfer is critical heat flux (CHF) threatening the uniformity of the system. If the CHF condition is reached, unwanted results such as sudden worsening of heat transfer between heating wall and coolant fluid, sharp decrease in heat transfer coefficient, and physical and chemical damage to the surface (fouling, fracture, etc.) appear, which might be dangerous for the safety of the system [13]. In the literature, extensive research for extending CHF has been conducted by means of micro/nanoscale surface enhancements and modification techniques [14–29].

Hwang and Kaviany [14] investigated the effects of uniform porous coatings on CHF enhancement. Copper particles, whose diameters were 40 and 80 μm, were used as coatings with different thicknesses (3 and 5 particle diameters), which significantly increased CHF (about 80%). Sarwar et al. [15] provided Al_2O_3 microporous coatings with particles having sizes smaller than 10 μm and coating thicknesses of 50 μm. A 25% increase in CHF was obtained. Khanikar et al. [16] utilized carbon nanotubes (CNTs) coatings onto rectangular microtubes to obtain CHF enhancement. The results indicated that CNT coating was a strong alternative for enhancing the boiling curve. Nevertheless, repetitions of tests resulted in damage in CNTs' morphology so that CHF enhancement lost its effect with increasing number of tests. Jeong et al. [17] used surfactant solutions (trisodium phosphate (TSP, Na_3PO_4, $12H_2O$)) for surface modification. CHF enhancement was tested at various mass fluxes (100–500 kg/m^2 s), and a 48% increase in CHF was obtained. Kim and Kim [18] used different nanoparticles (TiO_2, Al_2O_3, and SiO_2) to investigate flow boiling CHF of aqueous nanofluids. The experiments indicated that CHF was increased when nanoparticles were included in the working fluid. The main reason for CHF enhancement in nanofluids was observed to be nanoparticle deposition after the experiments. In other words, nanoparticles in nanofluids were deposited to the heater surface, and the resulting nanoparticle coating on heater surface altered the surface properties such as surface wettability, surface roughness, and maximum capillary wicking height. Şeşen et al. [19] investigated pool boiling on a plate having a planar copper thin film coated on a silicon wafer surface, on which an array of copper nanorods with an average diameter ∼100 nm and length ∼500 nm was integrated. They found that using nanostructured surfaces can have the potential to be an effective method of device cooling for small and excessive heat generating microsystem applications due to a significant increase in boiling heat transfer (more than 100%). For studying the effect of nanofluids on CHF enhancement, Kim et al. [20] tried to improve CHF by using Al_2O_3 nanoparticle based nanofluids. CHF of Al_2O_3 nanoparticle based nanofluids was greater than CHF of the pure based fluid (up to 70% increase). To observe the effects of graphene/graphene-oxide nanosheets, Park et al. [21] used graphene/graphene-oxide nanosheets as an additive in nanofluids. The experiments showed that these nanosheets extended boiling curves. Interestingly, the reason was attributed to neither improved surface wettability nor the capillarity of the nanoparticles deposition layer. This increase was explained by formation of self porous surface structure of graphene/graphene-oxide nanosheets. Forrest et al. [22] accomplished silica nanoparticle thin film coatings on nickel wire. The experiments showed that coating the nickel wire with silica nanoparticles was a successful method for enhancing CHF (up to 100%). Surface characterization results

[1]Corresponding author.

Contributed by the Heat Transfer Division of ASME for publication in the Journal of Heat Transfer. Manuscript received September 16, 2013; final manuscript received March 28, 2014; published online May 2, 2014. Assoc. Editor: W. Q. Tao.

indicated that surface wettability was drastically altered with the addition of silica nanoparticles, and CHF was positively affected by this surface modification. Morshed et al. [23] conducted their experiments with copper nanowire (CuNW) coatings on microtubes with a hydraulic diameter of 672 μm. Nanowires on the bottom surface of the microtube were deposited by using the electrochemical deposition technique. Boiling heat transfer experiments at various mass fluxes and subcoolings showed that the coating of CuNW in microtubes improved boiling heat transfer coefficient up to ~56%. For observing the effect of surface wettability on CHF, Phan et al. [24] prepared silicon oxide (SiO), titanium (Ti), diamond-like carbon, and carbon-doped silicon oxide surfaces, whose static contact angles were 26 deg, 49 deg, 63 deg, and 104 deg in a single rectangular channel having a height of 0.5 mm, a width of 5 mm and a length of 180 mm, respectively. The experiments conducted at the mass flux of 100 kg/m^2 s indicated that extended boiling curves could be obtained from surfaces, which had lower static contact angles. Ahn et al. [25] used zircaloy-4 micro/nanostructures to enhance CHF under different experimental conditions. Their results indicated that CHF in the annular flow regime might be significantly enhanced by high wettability of zircaloy-4 micro/nanostructures because of the increase in stability of the liquid film and better liquid replenishment as the mass flux increased. Betz et al. [26] investigated pool boiling on surfaces with various wettabilities (from superhydrophobic to superhydrophilic). They found that the highest heat transfer coefficients were reached on uniform surfaces with hydrophilic regions due to high wettability. Saeidi and Alemrajabi [27] investigated the effect of nanostructured surfaces on pool boiling by utilizing chromic acid and sulfuric acid solutions on aluminum. They found that critical heat flux could be increased by 8% compared to the untreated aluminum alloy surface. Moreover, boiling heat transfer coefficients were increased by 159% in weakly etched samples. Tang et al. [28] examined nucleate pool boiling heat transfer performance of a nanoporous copper surface fabricated by the facile hot-dip galvanizing process. They observed that the nanostructured surface reduced wall superheat and increased heat transfer coefficient compared to the unstructured surface at low heat flux conditions. Yongwei et al. [29] investigated pool boiling on coated surfaces with de-ionized water and saturated calcium carbonate solution. They found that pool boiling enhancement was observed with thinner nanoscale hydrophobic titania-fluoroalkylsilane composite films at higher heat fluxes compared to the thicker coating on stainless steel surfaces.

Encouraged by the abovementioned results with nanostructures and nanofilms deposited on various surfaces in boiling heat transfer, this experimental study examines a new technique for delaying DNB (departure from nucleate boiling) critical heat flux conditions and increasing subcooled boiling heat transfer in microtubes. Different from previous studies, this study includes the effects of coating thickness on flow boiling heat transfer enhancement in microtubes with crosslinked pHEMA coatings. Detailed discussion on the results along with performed visualization tests and enhancement mechanisms was given, thereby providing more physics and understanding. In this study, crosslinked polyhydroxyethylmethacrylate nanofilm coating, which is a type of hydrogels in aqueous medium, was applied to the inner walls of microtubes. pHEMA coating deposition is an important alternative method for enhancing the surface of microtubes/tubes. pHEMA could be coated with iCVD method, which is a simple to use, efficient, cheap, and uniform coating method, and is independent of surface shape. Furthermore, iCVD is one of the most suitable deposition technique for closed geometries such as microtubes, where physical deposition methods could not be implementable. In this study, the effect of thickness of swellable polymer crosslinked pHEMA coatings on CHF and boiling heat transfer enhancement was studied. The experiments were performed at two different mass fluxes, (5000 kg/m^2 s–20,000 kg/m^2 s). Crosslinked pHEMA was deposited on microtubes, whose inner diameters were 249 μm, 507 μm, and 908 μm. The pHEMA coating thicknesses were ~50 nm, 100 nm, and 150 nm, respectively.

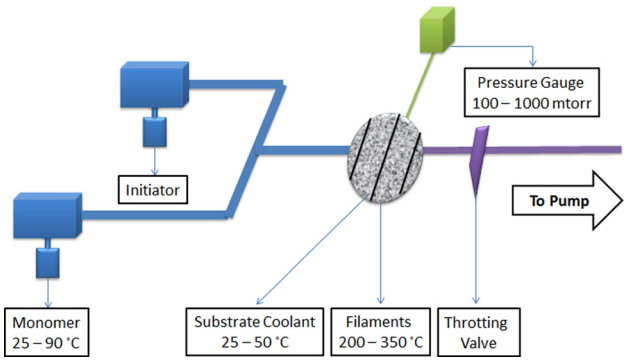

Fig. 1 Schematic of iCVD system and the components

pHEMA Deposition Method

pHEMA deposition is a difficult process since polymeric materials cannot be easily deposited onto substrates of complex structures and skinny regions. CVD method could supply enhanced uniformity and finely conserved coating clarity compared to other polymerization methods. CVD has several benefits when the coating is needed for the applications in microtubes. In this experimental study, it is not possible to apply solution polymerization methods to inner walls of the metal microtubes because liquid surface tension prevents uniformity and purity. On the other hand, solvents used in such methods may result in having residuals and additives, which could visibly break homogeneity of the coating [30]. For that reason, chemical vapor deposition may offer enhanced uniformity and pure coatings due to gas phase nature. iCVD is a novel technique used for deposition of polymeric thin films. Through iCVD, it can be achieved in one step of deposition for thin films of application-specific polymers without any liquid medium such as solvent. Also, the technique supplies low energy path for polymerization compared to common CVD techniques [31]. Even 3D structures could be coated with well uniformity and enhanced management on coating thickness by iCVD method. Moreover, iCVD is a kind of HWCVD (hot wire chemical vapor deposition), which is being increasingly used for the deposition of materials such as hydrogenated amorphous or microcrystalline silicon and its alloys and diamond films. The working principle of iCVD is based on the mechanism of free radical polymerization reaction. The system components are shown in Fig. 1.

The main part of the deposition system consists of a vacuum chamber evacuated by a pumping unit to some appropriate vacuum level. After achieving the desired ultimate vacuum, the process vapor mixture was introduced via mass flow controllers, and the pressure was kept constant by a variable conductance valve. The initiator vapor was then decomposed by the heat generated by a hot filament of tungsten, tantalum, or other material into radicals, which started the polymerization. Basically, the polymerization was performed in three steps: beginning phase, propagation, and finalization. At the beginning, initiator was fed into the system that was separated by heated filaments. The pressure varied between 10 and 130 Pa in the vacuum chamber. Crosslinker and monomer agents were heated to obtain the vapors to be delivered to the system. The radicals produced by heated filament attacked the adsorbed monomers on the substrate surface and initiated the polymerization. The surface was preserved at room temperature (around 22 °C), which raised the adsorption rate of gas phase molecules on the surface. On the other hand, filament temperature and substrate surface can be modified by different panels, and experimental conditions can be developed. iCVD was investigated for various materials and viscosity effects of the system pressure,

Table 1 Temperature, pressure, reactant function, and flow rate properties for iCVD deposition

	Reactant function	Flow rates, F (sccm)
TBPO	Initiator	1
EGDMA	Crosslinker	0.086
HEMA	Monomer	1.05
Nitrogen	Diluting element	
	Pm/Psat	Temperature (°C)	Total pressure (Torr)
TBPO	0.002	T_{diss}: 285	
EGDMA	0.299	T_h: 90	
HEMA	0.284	T_h: 80	
Nitrogen			0.20

filament temperature, stage temperature, feed rates of reactants could be simply conceived by different studies [32].

In this extensive experimental study, three different coating thicknesses were used for investigating the effect of coating thickness. Crosslinked pHEMA deposition durations were 45 min, 75 min, and 105 min for coating thicknesses of 50 nm, 100 nm, and 150 nm, respectively. In addition, hydrophobic crosslinker agent EGDMA was used to enhance mechanical strength of the polymer, which was essential for the films to survive the conditions in microtubes because pHEMA coated thin polymers films have weak mechanical features compared to common coatings. On the other hand, crosslink films increase the contact angle of deposited films (from 37 deg to 45 deg) with a crosslink ratio of 20% [33]. In addition, increased ratio of crosslink causes a decrease in the swelling proportion of thin films [34]. Hence, an optimized crosslink was required to establish stability between the mechanical strength and the swelling properties of the films. Table 1 displays experimental conditions for iCVD deposition of poly (HEMA-co-EGDMA) on the surfaces of microtubes.

The thickness of the nanofilm on inner walls of microtubes could not be directly measured due to low thickness of the polymeric thin film compared to that of the metal microtube. Instead, a silicon wafer, which was placed next to the microtube in the reactor during film deposition, was used for thickness and swelling measurements. Thickness measurements were done with regular mode of J.A Woollam VASE Ellipsometry. Since VASE is very sensitive to layer thickness down to subnanometer, it allows to measure thickness of thin films with an uncertainty of $\sim\pm5$ nm. With the information about thin film thickness of silicon wafer, the thickness of pHEMA coating can be then deduced. pHEMA is a polymer, which possesses the properties of hydrogels. One of these properties is high swelling ratio, which gives rise to a porous coating when being wetted. Thus, it is expected to see that thickness of pHEMA increases as working fluid is introduced to the microtube surface. The swelling ratio of the polymer coating was measured using Ellipsometry mentioned above. To check for this property, working fluid was dropped onto surface of the thin film and it is waited for 10 min to monitor a change in the thickness. The Ellipsometry results indeed showed that the thickness of HEMA-EGDMA thin film increased by ~21% validating the swelling property, which leads to a porous coating.

Experimental Setup and Procedure

The schematic of the setup is illustrated in Fig. 2. The test setup consists of the test section, a storage cylinder, an Omega® flow meter, a Xantrex XFR2800 power supply, multiple pressure sensors, thermocouples, and proper tubing and fittings. Figure 3 displays the schematic of the test section. Two alligator clips, which were specially shaped with machining tools to minimize the heated length and to reach a width of 1 mm, were attached to the microtube surface (with a 1 cm heated length). Alligator clips were assembled with a prescribed distance from each other and

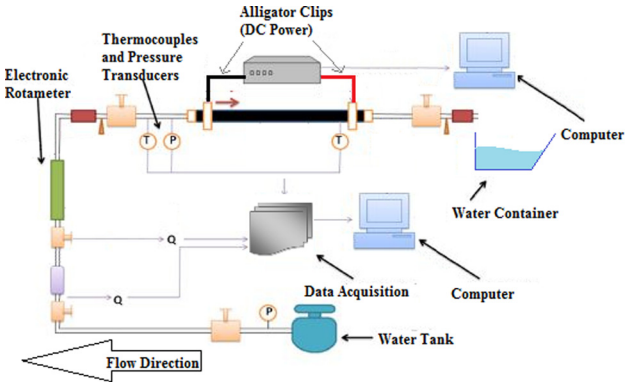

Fig. 2 Schematic of the heat transfer experiment setup

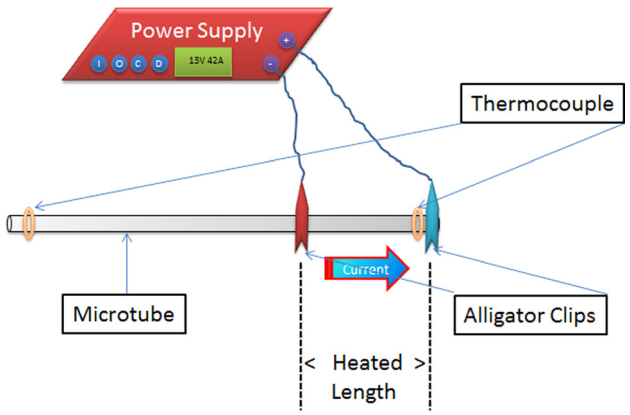

Fig. 3 Schematic of the test section

connected to the high current power supply, which supplies an adjustable dc current and high power input to provide Joule heating to the desired sections of ~4 cm long microtubes of 249 μm, 507 μm, and 908 μm inner diameters.

Conax® packing glands offer sealing between the microtube and the experimental loop. The test section was connected to the setup from the inlet side, whereas the outlet side was exposed to the atmosphere in order to guarantee atmospheric conditions at the outlet (exit) side. Moreover, one of Omega® thermocouples was assembled upstream the inlet of microtube in order to investigate bulk temperatures at the inlet. Pressure measurements were performed via Omega® pressure transducers with various ranges (between 0 and 3000 psi gauge pressure). Inlet pressures varied from 122 to 1552 kPa. An Omega® turbine meter was used to collect flow rate data, which were obtained together with the voltage and current data. Collected data were transferred to the computer for data reduction. Local surface temperature at the outlet of the tube was measured via a thin Omega® thermocouple wire (~76 μm thick). This thermocouple was connected to the microtube surface at the end of the heated length of the microtube, where the maximum temperature was expected along the test section via Omega® Bond and atmospheric conditions are present. Exit mass qualities vary from −0.079 to −0.147 in this study.

During the experiments, the flow rate was fixed at the desired value by tuning the pressure difference between microtube inlet and exit. The temperature and pressure data were obtained from the Labview® interface. The experiments were performed under steady state conditions. By adjusting the current from power supply, the power was increased by up to ~0.5 Amps increments until the test setup lost its uniformity because of extreme overheating conditions (CHF condition). This procedure was repeated for different mass fluxes. De-ionized water was utilized as working fluid, and inlet fluid temperature was the ambient temperature.

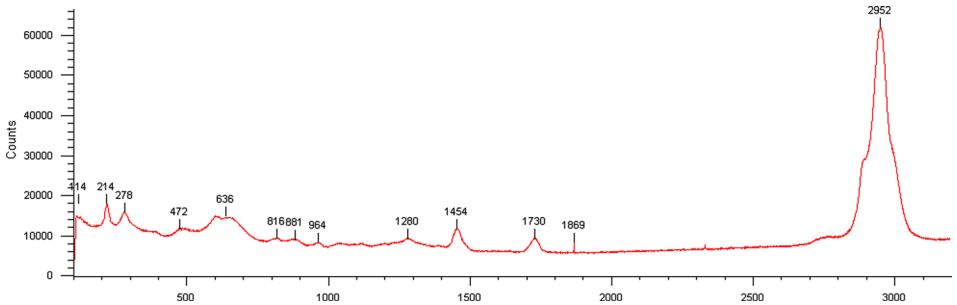

Fig. 4 Raman spectrum taken from the inner surface of the untreated sample microtube having 249 μm inner diameter

In our previous experimental studies, the experimental setup was validated with single-phase heat transfer tests [35,36]. In order to calculate approximate heat losses, power was applied to the test section following evacuating de-ionized water from the test section. The temperature difference between the test section and atmosphere was recorded with the corresponding current value after the surface temperature of the test section reached to steady conditions. Since power values and temperature differences were recorded simultaneously, power versus temperature difference profile could be obtained in order to calculate the heat loss corresponding to each experimental data point, and a heat loss calibration curve was obtained. Accordingly, the average heat loss was found to be 5.6%, and heat losses were taken into account in the data reduction.

Raman Spectroscopy Results

Raman spectroscopy is a kind of technique based on vibrational spectroscopy and is the most common spectroscopic technique used to assess molecular motion and fingerprinting species. Based on inelastic scattering of a monochromatic excitation source, routine energy range can be up to 200–4000 cm^{-1} [37]. Raman Spectrometry was used for the analysis of pHEMA coatings. Raman spectral analysis was conducted at the Renishaw inVia Raman Microscope attached with a 532 nm green laser and 2400 lines/mm grating. pHEMA coatings were tested apart from the experiments to investigate the strength and reliability. In Figs. 4 and 5, treated and nontreated plates were compared based on Raman spectrum. The pHEMA coated plates were exposed to very high temperature (255 °C) by heating the plate using a film heater for a time period of 87 min. Moreover, to observe the impact of pressurized water flows on pHEMA coatings, the pHEMA coated plate was manually subjected to water flow ($G = 5000–20{,}000\ kg/m^2\ s$ flowing inside 249 μm, 507 μm, and 998 μm microtubes) with the same mass fluxes as under the experimental conditions.

As seen in Fig. 5, pHEMA coating was present after the treatment due to a similar Raman spectrum compared to the untreated plate. Therefore, it was proven that pHEMA is reliable and sustainable method as a stable and durable coating alternative. According to Fig. 5, the biggest band appearing at 2952 cm^{-1} is due to the $\nu_{as}CH_2$ stretching mode [38]. It is known that between 2800 and 3100 cm^{-1} valence vibrations of CH_2 and CH_3 were becoming dominant [39]. The Raman peak located at 1454 cm^{-1} result from the deformation of C-H group. It is critical to analyze whether the spectrum contains any C=C related Raman peak. Because the polymer inside the tubes was deposited with free radial polymerization the C=C bonds were expected to be broken during the synthesis. HEMA produces two significant C=C related Raman peaks: 1280 cm^{-1} (C=CH_2 stretching vibration) and 1454 cm^{-1} (C=C aliphatic stretching vibration). The absence of these peaks proves that C=C bonds in the methacrylate group were opened forming pHEMA chains. Other peaks and corresponding modes were as follows: 1730 cm^{-1} (νC=O), 636 cm^{-1} (ν_sCCO), and 964 cm^{-1} (ρCH_3) (ν: stretching, ρ: rocking, s: symmetric, as: asymmetric) [40].

Crosslinking ratio of thin film was calculated with spectra of coated silicon wafer. Herein, it is necessary to have spectra of pure pHEMA and pHEMA-EGDMA. The calculation begins with the computation of the ratio (denoted as r) of the peak area of C=O stretching region (1730–1740 cm^{-1}) to O-H region (3000–3400 cm^{-1}) in pure pHEMA thin film. However, the normalization of the intensities in spectra is important to obtain the correct ratio. The normalization is done by dividing intensity of peaks to thickness of thin films. The normalization should be done for both pure HEMA and HEMA-EGDMA spectra. Then, it is necessary to find the area of C=O peak and O-H peak of HEMA-EGDMA to obtain crosslinking ratio. The following formula gives the ratio of crosslinking, where A_{CO} is area under carbonyl stretching peak and A_{OH} is area under hydroxyl peak:

$$\frac{\text{EGDMA}}{\text{HEMA}} = \frac{(A_{CO} - rA_{OH})/2}{rA_{OH}} \tag{1}$$

Data Reduction and Uncertainties

The voltage, current, flow rate, and temperature data are reduced to attain heat transfer coefficients and CHF.

The mass flux can be found using the following formula:

$$G = \dot{m}/A_c \tag{2}$$

where A_c is the cross section of the microtube.

CHF is expressed as

$$q''_{CHF} = \frac{(P - \dot{Q}_{loss})}{\pi d_i L_h} \tag{3}$$

where $(P - \dot{Q}_{loss})$ is the applied net power, d_i is the inner hydraulic diameter, and L_h is the heated length.

Two-phase heat transfer coefficient at the exit of the tube is expressed as

$$h_{tp} = \frac{(P - \dot{Q}_{loss})}{\pi d_i L_h (T_{w,i} - T_{sat})} \tag{4}$$

Assuming 1D steady state heat conduction with uniform heat generation, the local inner surface temperature of the microtube, $T_{w,i}$, is expressed in terms of the measured local outer surface temperature, $T_{w,o}$, as

$$T_{w,i} = T_{w,o} + \frac{\dot{q}}{4k_w}(r_o^2 - r_i^2) - \frac{\dot{q}}{2k_w} r_o^2 \log\left(\frac{r_o}{r_i}\right) \tag{5}$$

where k_w is heat thermal conductivity of the wall, r_o is outer radius of the microtube, r_i is inner radius of the microtube, and $\dot{q}$ is the volumetric heat generation. $\dot{q}$ is expressed as a function of net

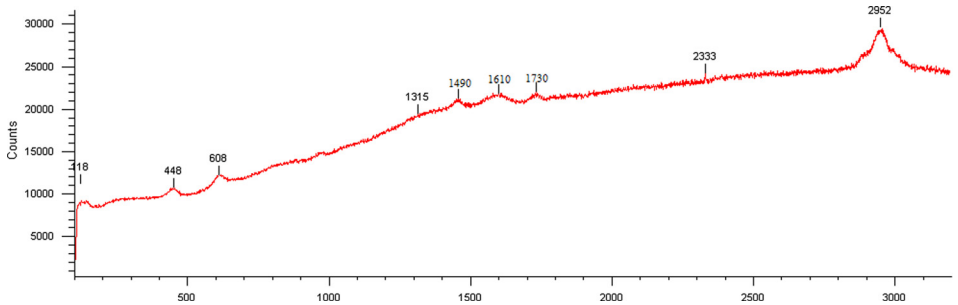

Fig. 5 Raman spectrum taken from the inner surface of the treated sample microtube having 249 μm inner diameter

Table 2 Uncertainties in experimental parameters

Parameter	Uncertainty
Inner diameter, d_i	$\pm 2\,\mu$m
Temperature, T	± 0.1 °C
Electrical power, P	$\pm 0.2\%$
Heat flux, q''	$\pm 3.2\%$
Mass flux, G	$\pm 2.6\%$
Two-phase heat transfer coefficient, h_{tp}	$\pm 12.2\%$
Coating thickness	± 5 nm

power, inner microtube radius, outer microtube radius, and heated length as

$$\dot{q} = \frac{(P - \dot{Q}_{loss})}{\pi(r_o^2 - r_i^2)L_h} \tag{6}$$

Local exit mass quality was deduced based on energy balance

$$x_e = \frac{q''\pi d_i L_h - \dot{m}c_{p,e}(T_{sat,e} - T_i)}{\dot{m}h_{FG,e}} \tag{7}$$

where $\dot{m}$ is mass flow rate, c_p is specific heat, T_i is inlet temperature, and h_{FG} is latent heat of vaporization.

The uncertainties in the measured values are given in Table 2. They were obtained using the propagation of uncertainty method developed by Kline and McClintock [41].

Results and Discussion

Before boiling heat transfer tests, single-phase pressure drop tests under the same mass fluxes ($G = 5000$ and 20,000 kg/m^2 s) for all used microtubes were conducted and the results were validated with single-phase correlations with friction factor results. Pressure drops are 110.9, 48.8, and 21 kPa at the mass flux of 5000 kg/m^2 s for the tubes of inner diameters of 249 μm, 507 μm, and 998 μm, respectively, while they are 1451.9, 566, and 241.8 kPa at the mass flux of 20,000 kg/m^2 s for the tubes of inner diameters of 249 μm, 507 μm, and 998 μm, respectively. There is a good agreement between experimental results and available correlations (Colebrook correlation [42] for turbulent flow conditions (Re > 2300), $f = 64/\text{Re}$ for laminar flow conditions (Re < 2300)) (Fig. 6). All of the experimental data fall within ± 15% of the predicted values. In previous studies of the authors [43,44], single-phase heat transfer results on similar microtube configurations were found to be close to the theoretical predictions from available correlations under similar experimental conditions for the single-phase flow, which serves for another validation of the current experimental setup.

During the experiments, it was observed that there is a weak dependency of pressure drop on the heat flux. Thus, pressure drops in the boiling zone near the CHF condition are close to pressure drops under adiabatic conditions (typically 10–20% higher). The observations agree with the results in literature on pressure drop in subcooled boiling [45,46]. Tarasova et al. [45] correlation recommended for pressure drop in subcooled boiling predicts a minor change, while Dormer and Bergles [46] reported that the pressure drop dependency on heat flux diminishes in subcooled boiling with the decrease in the channel size.

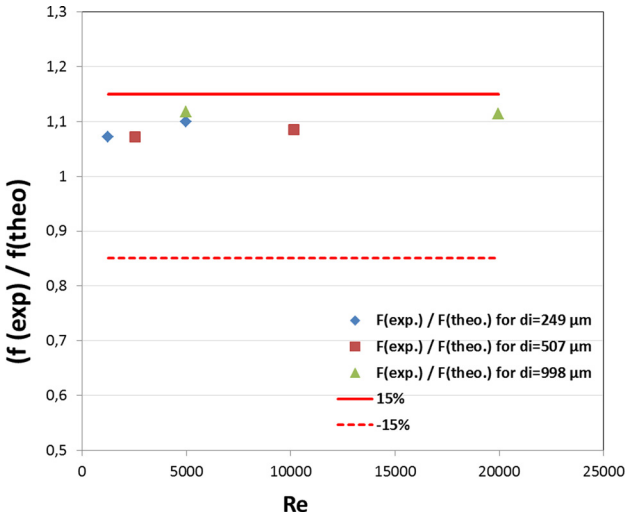

Fig. 6 *f*(experimental)/*f*(theoretical)—Reynolds number profile

Due to high mass fluxes in this study, corresponding Reynolds numbers are also high (Re > 1000). In the literature, it was reported that for high Re numbers (Re > 1000) axial conduction effects are negligible [47,48]. Thus, no significant axial conduction effects are expected in this study.

Boiling Curves. In Fig. 7, boiling curves for noncoated and crosslinked pHEMA coated microtubes having an inner diameter of 249 μm with coating thicknesses of ~50 nm, 100 nm, and 150 nm were shown at the mass flux of 5000 kg/m^2 s.

The largest CHF enhancement is observed at the pHEMA coated microtube having the thickest coating (~150 nm). Compared to the noncoated microtube, maximum enhancement is around 20.4%, while enhancements are 17.3% and 13.2% for coating thicknesses of 50 nm and 100 nm, respectively. In the relevant literature, it was found that contact angle decreases with the increase in nanostructure coating thickness [49]. Accordingly, lower contact angle promotes wetting [50]. Moreover, surface characteristics are also considerably changed with pHEMA coating since thicker coatings result in more porous structure.

In Fig. 8, identical crosslinker configurations are used for investigating CHF enhancements on microtubes of a diameter of 507 μm at the mass flux of 5000 kg/m^2 s. Similar trends in boiling curves can be observed. CHF enhancement ratios are less than

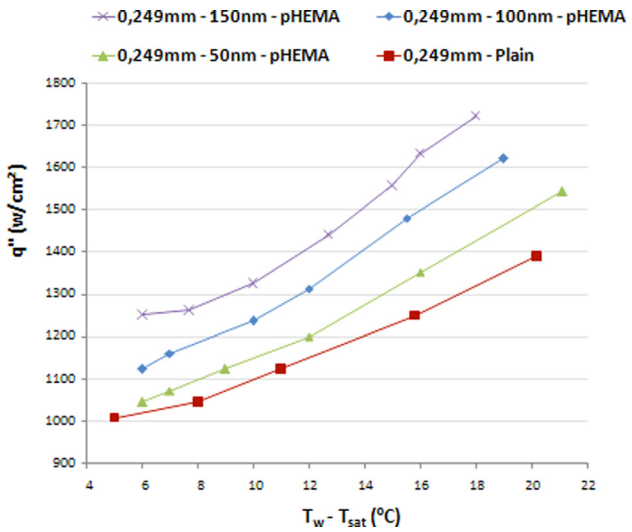

Fig. 7 Boiling curves for plain surface microtubes and pHEMA coated microtubes (50 nm, 100 nm, and 150 nm thick coatings) with an inner diameter of 249 μm at the mass flux of 5000 kg/m^2 s

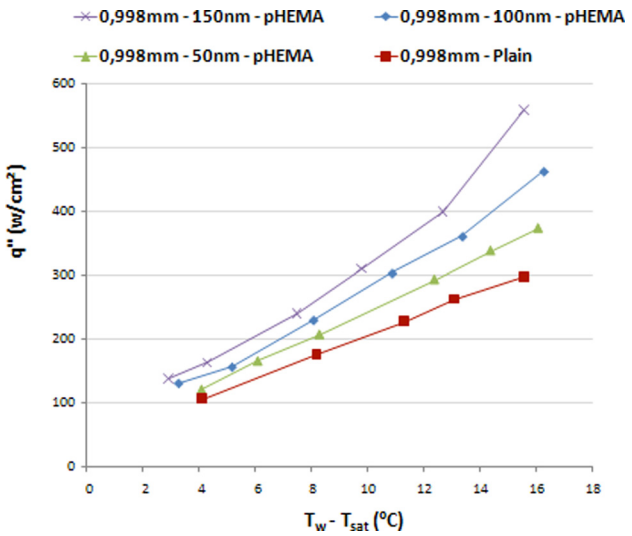

Fig. 9 Boiling curves for plain surface microtubes and pHEMA coated microtubes (50 nm, 100 nm, and 150 nm thick coatings) with an inner diameter of 998 μm at the mass flux of 5000 kg/m^2 s

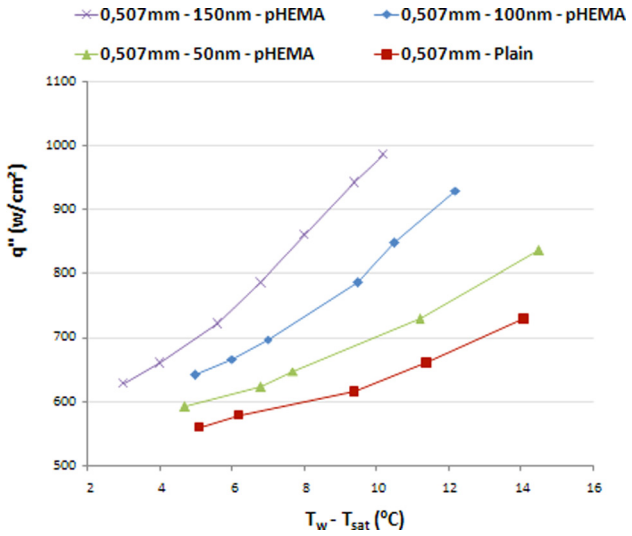

Fig. 8 Boiling curves for plain surface microtubes and pHEMA coated microtubes (50 nm, 100 nm, and 150 nm thick coatings) with an inner diameter of 507 μm at the mass flux of 5000 kg/m^2 s

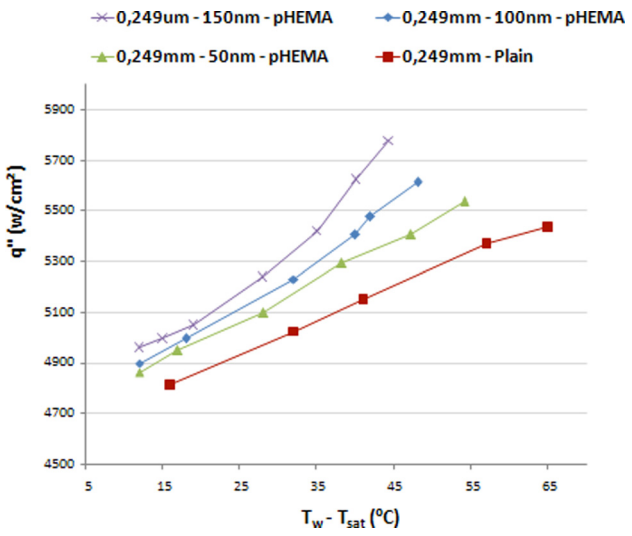

Fig. 10 Boiling curves for plain surface microtubes and pHEMA coated microtubes (50 nm, 100 nm, and 150 nm thick coatings) with an inner diameter of 249 μm at the mass flux of 20,000 kg/m^2 s

those corresponding to the microtube of diameter of 249 μm. CHF enhancements in this case are 10.1%, 14%, and 15.3% for coating thicknesses of 50 nm, 100 nm, and 150 nm, respectively.

The boiling curves for the microtube having an inner diameter of 908 μm are displayed in Fig. 9. Accordingly, the same trends related to coating thickness as in other cases can be noted in boiling curves. pHEMA coatings result in enhancement ratios of 8.9%, 11% and 12.5% for coating thicknesses of 50 nm, 100 nm, and 150 nm, respectively.

Figures 10–12 show boiling curves at the mass flux of 20,000 kg/m^2 s. As can be seen from these figures, the highest enhancement in CHF occurs in the microtube having the smallest diameter. Moreover, the highest CHF enhancement is observed in the microtube with the thickest pHEMA coating in this case. The CHF enhancement ratios are 29.7%, 26%, and 23.1% for coating thicknesses of 50 nm, 100 nm, and 150 nm, respectively. As shown in Figs. 11 and 12, similar trends are present for the microtubes having 507 μm and 908 μm inner diameters. The maximum CHF enhancement ratio is found as 24.8% in the microtube having an inner diameter of 507 μm and corresponds to the thickest pHEMA coating, while the maximum enhancement ratio is 20.1% in the microtube having an inner diameter of 908 μm for the thickest coating.

Swelling property and smaller contact angle result in CHF improvement in coated tubes. This effect is more dominant for the thickest coating configuration. The contact angle is approximately 75 deg between water and noncoated microtube wall, while the contact angle is about 45 deg between water and crosslinked pHEMA coated inner surface. Crosslinked pHEMA coating also results in extra wetting layer on inner microtube walls [51], which can be extended with thicker coatings. For enhanced surfaces, where passive enhancement is performed, suction-evaporation mode exists at higher heat fluxes [52]. In this mode, it was reported that the liquid is sucked through the porous layer on the enhanced surface through inactive pores. Then, this sucked liquid spreads and evaporates from active pores [53]. This mechanism for enhancement is amplified by the capillary-porous structure and

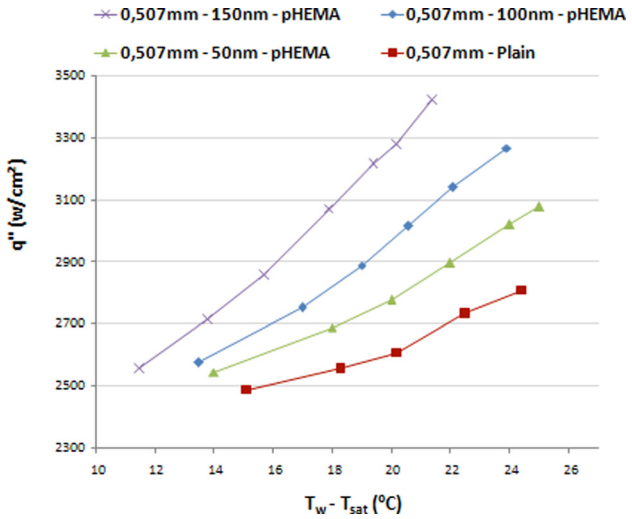

Fig. 11 Boiling curves for plain surface microtubes and pHEMA coated microtubes (50 nm, 100 nm, and 150 nm thick coatings) with an inner diameter of 507 μm at the mass flux of 20,000 kg/m^2 s

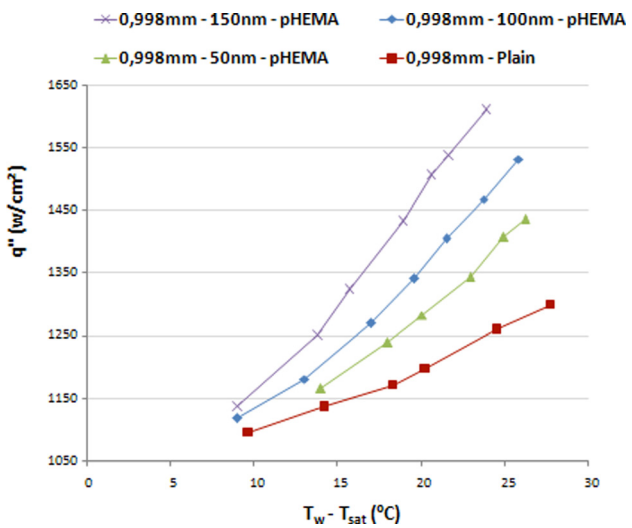

Fig. 12 Boiling curves for plain surface microtubes and pHEMA coated microtubes (50 nm, 100 nm, and 150 nm thick coatings) with an inner diameter of 998 μm at the mass flux of 20,000 kg/m^2 s

structural parameters such as the coating thickness and porosity. Since crosslinked pHEMA coating offers a highly capillary-porous structure, which is improved with an increase with the coating thickness, CHF condition is delayed with an increase with pHEMA coating thickness [54].

According to the results, it is found that CHF considerably decreases when the microtube diameter increases. Previous studies have similar findings regarding the effects of diameter [36,55,56]. Increased bubble velocity relative to the bulk fluid and condensation effects in smaller diameter channels result in an increase in CHF [56]. Moreover, the length of heated tube is significantly large compared to the tube diameter. It is proven that the emerging bubbles occupy a bigger portion of the microtube cross-section especially for small diameters [57]. This interaction between the fluid flow and emerging bubbles may have an effect on flow boiling leading to significant diameter effects on CHF compared to bigger size channels. It can be clearly seen that mass flux has significant effects on CHF according to the experimental results. CHF has an increasing trend with mass flux. In the previous studies, mass flux effects on CHF were investigated, and it was found that there was an increasing trend in CHF with the mass flux [1,58–60]. Growing bubbles, bubbles crowding channel surfaces, and slugs or vapor clots are possible scenarios for triggering DNB type CHF conditions [61]. Since they can be more easily removed at higher flow rates and more effective liquid replenishment to the tube wall occurs, CHF condition is delayed to higher heat flux values. CHF has a linear and stronger relationship with mass flux in contrast to conventional channel results [62], which might be explained by possible bubble-to-channel interactions reported in the literature [63].

Heat Transfer Results. Figures 13(*a*)–13(*c*) and 14(*a*)–14(*c*) display experimental two-phase heat transfer coefficient profiles at different microtube sizes (249 μm, 507 μm, and 908 μm) and mass fluxes ($G = 5000$ kg/m^2 s and $G = 20{,}000$ kg/m^2 s).

In Figs. 13(*a*)–13(*c*), two-phase heat transfer coefficients are displayed at the mass flux of 5000 kg/m^2 s for the microtubes having diameters of 249 μm, 507 μm, and 908 μm, respectively. According to the results, local two-phase heat transfer coefficient ($h_{\text{tp-local}}$) considerably increases with pHEMA coating, and it has an increasing trend with the pHEMA coating thickness.

Two-phase heat transfer coefficient enhancements up to 97.4% are obtained in the microtube having the smallest diameter with the thickest configuration, which is because high crosslinker coating thickness leads to an increase in nucleation site density due to more porous structure and to an increase in bubble generation frequency. Boiling heat transfer (at a fixed heat flux) enhancements up to 85% and 77.1% are obtained at the mass flux of 5000 kg/m^2 s for the microtubes of inner diameters of 507 μm and 908 μm, respectively. The largest enhancements are again obtained from the thickest crosslinked pHEMA coated tube configurations.

In Figs. 14(*a*)–14(*c*), two-phase heat transfer coefficients are shown as a function of heat flux performed for microtubes of different inner diameters (249 μm, 507 μm, and 908 μm) and coating thicknesses (50 nm, 100 nm, and 150 nm) at the mass flux of $G = 20{,}000$ kg/m^2 s. Similar trends in $h_{\text{tp-local}}$ compared to Figs. 13(*a*)–13(*c*) are observed at this mass flux value. As expected, the highest enhancements are attained from the smaller size microtube and the thickest coating. Enhancement ratios in boiling heat transfer coefficients up to 126.2% are obtained in the smallest size microtube (of diameter of 249 μm), while maximum enhancements in boiling heat transfer coefficients are 90.1% and 86.4% for the microtubes of 507 μm and 908 μm inner diameters, respectively.

In the literature, the advantages of nanostructure coating and deposition on boiling heat transfer were extensively discussed [64,65]. The underlying mechanism for enhanced boiling heat transfer performance with crosslinked pHEMA coating may be attributed to its ability of increasing the nucleation site density by providing more active nucleation sites because of its very porous structure and by enhancing incidence of bubble occurring from surface which is more dominant for thicker coatings.

In the visualization tests, the applied heat flux was fixed to 40 W/cm^2 for both noncoated and pHEMA coated plate surfaces, which were heated by cartridge heaters in a pool with transparent sides (Fig. 15). A Phantom V310 high speed camera was used for this task, while the image resolution, sample rate, and exposure time were 1200 × 800 pixels, 2800 fps, and 100 μs, respectively. Images were recorded for approximately 60 s for an applied heat flux, which was selected to monitor the performance of the plates at the isolated bubble regimes.

In order to observe plates from the lateral side, the experimental setup made of glass was prepared. An aluminum base (19 mm × 19 mm) was constructed for a cartridge heater of length of 19.25 mm and of a diameter of 4.5 mm. The base was also surrounded with glass walls with height of 20 cm to have a similar shape as pool. To prevent any leakage, the setup was sealed with liquid gasket. Moreover, pHEMA and noncoated plates were

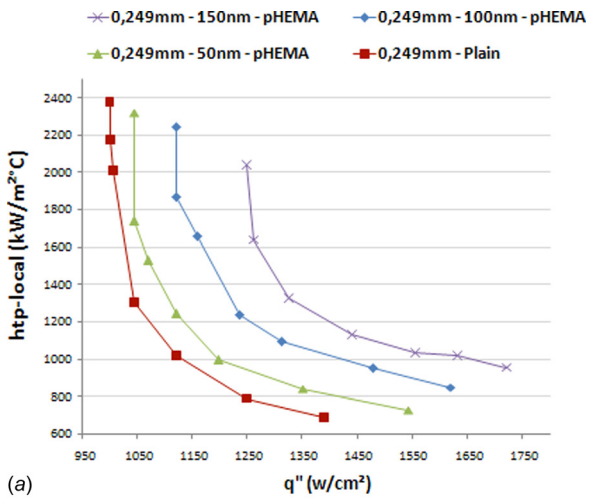

(*a*)

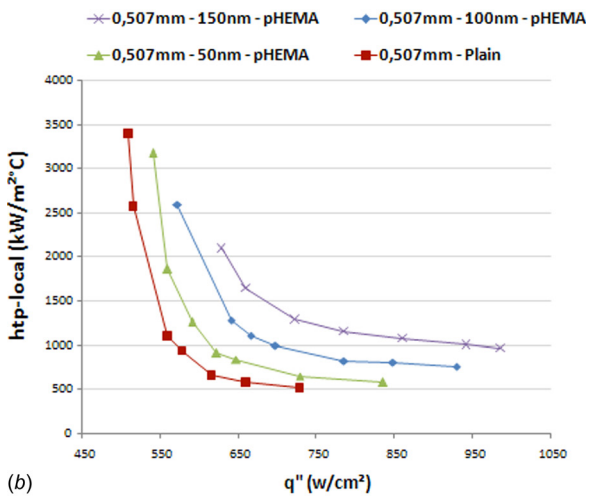

(*b*)

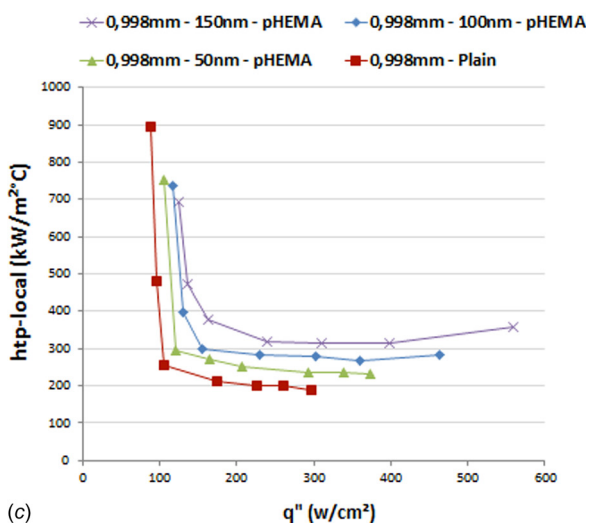

(*c*)

Fig. 13 (*a*) Two-phase heat transfer coefficient for plain surface microtubes and pHEMA coated microtubes (50 nm, 100 nm, and 150 nm thick coatings) with an inner diameter of 249 μm at the mass flux of 5000 kg/m^2 s. (*b*) Two-phase heat transfer coefficient for plain surface microtubes and pHEMA coated microtubes (50 nm, 100 nm, and 150 nm thick coatings) with an inner diameter of 507 μm at the mass flux of 5000 kg/m^2 s. (*c*) Two-phase heat transfer coefficient for plain surface microtubes and pHEMA coated microtubes (50 nm, 100 nm, and 150 nm thick coatings) with an inner diameter of 998 μm at the mass flux of 5000 kg/m^2 s.

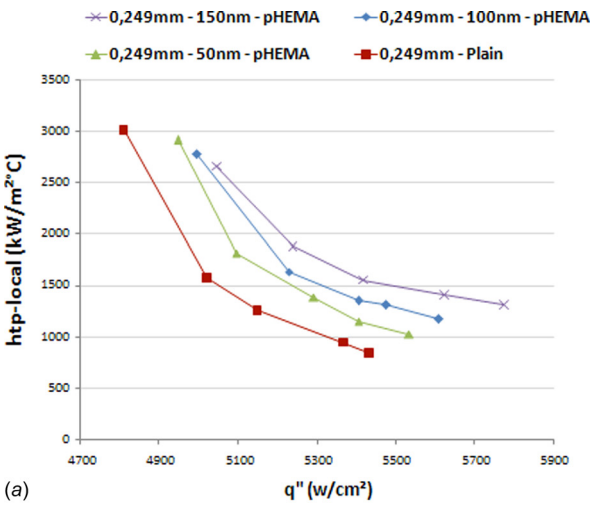

(*a*)

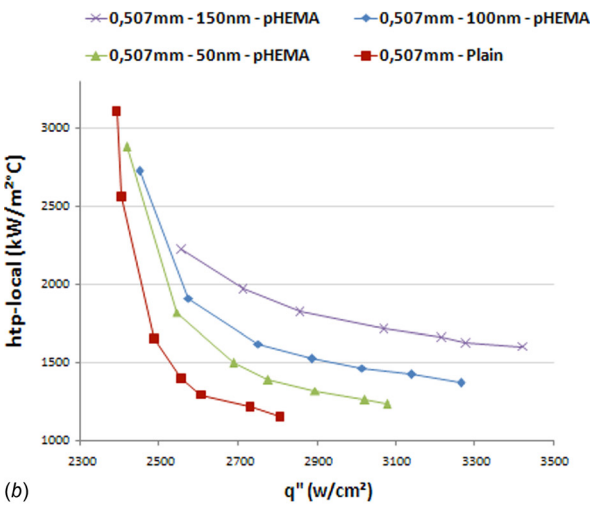

(*b*)

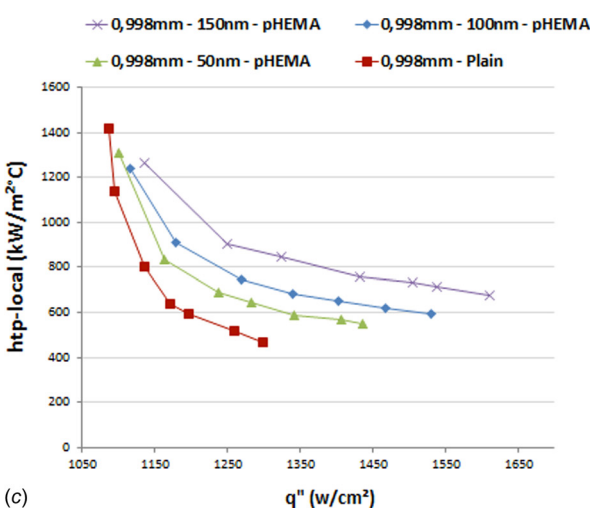

(*c*)

Fig. 14 (*a*) Two-phase heat transfer coefficient for plain surface microtubes and pHEMA coated microtubes (50 nm, 100 nm, and 150 nm thick coatings) with an inner diameter of 249 μm at the mass flux of 20,000 kg/m^2 s. (*b*) Two-phase heat transfer coefficient for plain surface microtubes and pHEMA coated microtubes (50 nm, 100 nm, and 150 nm thick coatings) with an inner diameter of 507 μm at the mass flux of 20,000 kg/m^2 s. (*c*) Two-phase heat transfer coefficient for plain surface microtubes and pHEMA coated microtubes (50 nm, 100 nm, and 150 nm thick coatings) with an inner diameter of 998 μm at the mass flux of 20,000 kg/m^2 s.

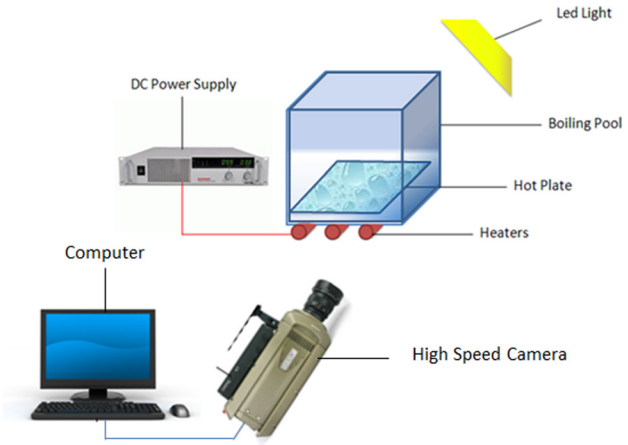

Fig. 15 The schematic of the experimental setup for visualization

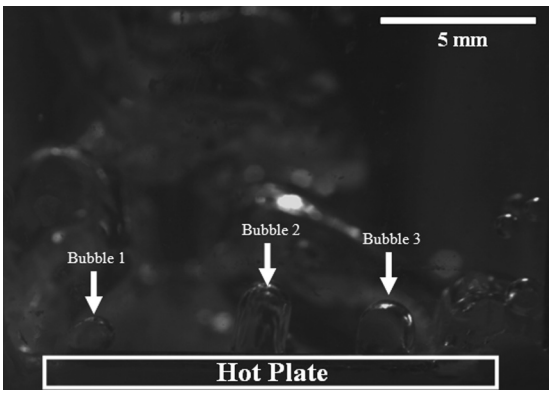

Fig. 16 Bubbles emerging from the noncoated plate

placed at on the surface of the bottom of aluminum base with Omega® Bond thermal grease.

For determining the average bubble departure frequency from the plates, the total number of emerged bubbles from plates was counted and averaged over monitoring time. Average bubble departure diameter from both pHEMA and noncoated plates was calculated by measuring the diameter of each bubble individually and averaging the sum of all diameters over the total number of emerged bubbles. The reliability of data was proven with long recording time since a cycle of bubble growth and release has an order of magnitude of milliseconds.

Figures 16 and 17 displaying bubbles emerging from noncoated and pHEMA coated (with a coating thickness of 150 nm) surfaces. As can be seen from the figures, at 40 W/cm^2 heat flux (at ~9.5 K wall superheat) more individual bubbles emerged for the pHEMA coated plate (~3 and ~7 bubbles were emerging on average from 1 cm^2 hot plate for noncoated and pHEMA coated plates, respectively). The duration of a bubble growth cycle is also shorter for the pHEMA coated surface (~10 ms) compared to the noncoated surface (~50 ms). The bubble departure diameters are ~2 mm and ~4 mm for noncoated and pHEMA coated plates, respectively. From the figures, it is clear that pHEMA coated plate increases the number of the nucleation site significantly compared to noncoated plate, and these figures serve as a proof of boiling heat transfer enhancement on coated surfaces.

The results prove that crosslinked pHEMA coatings improve boiling heat transfer for microscale cooling applications, where enhancement may be not possible with common surface enhancement and microfabrication methods. This method may provide a

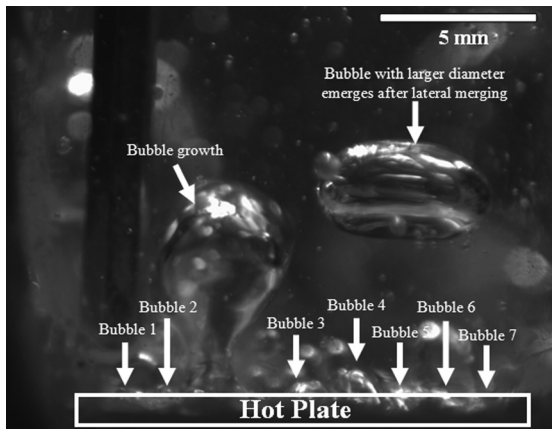

Fig. 17 Bubbles emerging from the crosslinked pHEMA coated plate

feasible solution, when geometrical modifications are not possible with physical deposition methods in cases such as closed geometries.

Conclusions

In this study, flow boiling heat transfer performance was investigated in microtubes with different crosslinked pHEMA coating thicknesses (50 nm, 100 nm, and 150 nm) and in plain microtubes having inner diameters of 249 μm, 507 μm, and 908 μm at mass fluxes of 5000 kg/m^2 s and 20,000 kg/m^2 s. Significant increase in CHF and heat transfer coefficient with crosslink pHEMA coatings was obtained. The major findings of this study are as follows:

- The swelling property of the pHEMA coatings has a positive effect on CHF due to the resulting increase in surface wettability.
- Larger coating thicknesses result in larger increase in CHF.
- Crosslinked pHEMA coating improves boiling heat transfer performance since it increases the nucleation site density by offering more active nucleation sites due to its porous structure, raises bubble generation frequency from the surface, and improves liquid replenishment to the surface after bubble departures. This effect is more pronounced for thicker coatings.
- iCVD was proven to be a practical method for pHEMA coatings in microscale channels/tubes, in which the application of existing conventional methods is limited.
- The results were supported by the visualization tests performed on both plain and pHEMA coated rectangular plates.

Acknowledgment

The authors would like to thank the Sabancı University Nanotechnology Research and Application Center (SUNUM) for the continued equipment and characterization support. This work was supported by Turkish Scientific Council, Grant No. 112M940 and TUBA (Turkish Academy of Science) Outstanding Young Investigator Support Program (GEBIP). Graduate student support provided by the Faculty of Engineering and Natural Sciences of Sabancı University is greatly appreciated. In addition, Dr. Meltem Sezen's assistance in Raman spectroscopy is highly appreciated.

Nomenclature

A_c = cross-sectional area, m^2
c_p = specific heat of water, kJ kg^{-1} °C^{-1}
d_i = channel inner diameter, M
G = mass flux, kg m^{-2} s^{-1}
h_{FG} = latent heat of vaporization, J kg^{-1} K^{-1}

h_{tp} = boiling heat transfer coefficient, W cm^{-2} K^{-1}
L_h = heated length, M
$\dot{m}$ = mass flow rate, kg s^{-1}
p = pressure, Pa
P = electrical power, W
q'' = heat flux, W cm^{-2}
$\dot{q}$ = volumetric heat generation, W m^{-3}
$\dot{Q}_{loss}$ = heat loss, W
T_{diss} = dissociation temperature, °C
T_h = heating temperature of monomer, °C
T_i = inlet temperature
T_{sat} = saturation temperature, °C
$T_{w,i}$ = inner wall temperature, °C
$T_{w,o}$ = outer wall temperature, °C
x_e = exit mass quality,

Subscripts

CHF = critical heat flux
e = exit
h = heated
i = inlet, inner
sat = value at saturation
w = wall

References

[1] Koşar, A., 2009, "A Model Predict Saturated Critical Heat Flux in Minichannels and Microtubes," Int. J. Therm. Sci., **48**(2), pp. 261–270.
[2] Koşar, A., Schneider, B., and Peles, Y., 2007, "Hydrodynamic Cavitation and Boiling in Refrigerant (R-123) Flow Inside Microtubes," Int. J. Heat Mass Transfer, **50**(13-14), pp. 2828–2854.
[3] Koşar, A., and Peles, Y., 2007, "Critical Heat Flux of R-123 in Silicon-Based Microtubes," ASME J. Heat Transfer, **129**(7), pp. 844–851.
[4] Kandlikar, S. G., 2002, "Fundamental Issues Related to Flow Boiling in Minichannels and Microtubes," Exp. Therm. Fluid Sci., **26**(2-4), pp. 389–407.
[5] Lin, L., 1998, "Microscale Thermal Bubble Formation: Thermophysical Phenomena and Applications," Microscale Thermophys. Eng., **2**(2), pp. 71–85.
[6] Yu, W., France, D. M., Wambsganns, M. W., and Hull, J. R., 2002, "Two-Phase Pressure Drop Boiling Heat Transfer and Critical Heat Flux to Water in a Small-Diameter Horizontal Tube," Int. J. Multiphase Flow, **28**, pp. 927–941.
[7] Tran, N. T., Chyu, M. C., Wambsganss, W. M., and France, D. M., 2000, "Two Phase Pressure Drop of Refrigerants During Flow Boiling in Small Channels: An Experimental Investigation and Correlation Development," Int. J. Multiphase Flow, **26**(11), pp. 1739–1754.
[8] Ribatski, G., Wojtan, L., and Thome, J. R., 2006, "An Analysis of Experimental Data and Prediction Methods for Two-Phase Frictional Pressure Drop and Flow Boiling Heat Transfer in Micro-Scale Channels," Exp. Therm. Fluid Sci., **31**(1), pp. 1–19.
[9] Thome, R. J., 2004, "Boiling in Microtubes: A Review of Experiment and Theory," Int. J. Heat Fluid Flow, **25**(2), pp 128–139.
[10] Bertsch S. S., Groll, E. A., and Suresh V. G., 2008, "Review and Comparative Analysis of Studies on Saturated Flow Boiling in Small Channels," Nanoscale Microscale Thermophys. Eng., **12**(3), pp. 187–227.
[11] Kaya, A., Ozdemir, M. R., and Kosar, A., 2013, "High Mass Flux Flow Boiling and Critical Heat Flux in Microscale," Int. J. Therm. Sci., **65**, pp. 70–78.
[12] Koşar, A., Peles, Y., and Bergles, A. E., 2009, "Experimental Investigation of Critical Heat Flux in Microtubes for Flow-Field Probes," ASME 7th ICNMM Conference, Pohang, South Korea, June 22–24.
[13] Kandlikar, S. G., Shoji, M., and Dhir, V, K., 1999, *Handbook of Phase Change*, Taylor & Francis, New York.
[14] Hwang, G. S., and Kaviany, M., 2006, "Critical Heat Flux in Thin, Uniform Particle Coatings," Int. J. Heat Mass Transfer, **49**(5–6), pp. 844–849.
[15] Sarwar, M. S., Jeong, Y. H., and Soon, H. C., 2007, "Subcooled Flow Boiling CHF Enhancements With Porous Surface Coatings," Int. J. Heat Mass Transfer, **50**, pp. 3649–3657.
[16] Khanikar, V., Mudawar, I., and Fisher, T., 2009, "Effects of Carbon Nanotube Coating on Flow Boiling in a Microtube," Int. J. Heat Mass Transfer, **52**, pp. 3805–3817.
[17] Jeong, H. Y., Sarwar, S. M., and Chang, H. S., 2008, "Flow Boiling CHF Enhancement With Surfactant Solutions Under Atmospheric Pressure," Int. J. Heat Mass Transfer, **51**(7–8), pp. 1913–1919.
[18] Kim, H., and Kim, M., 2009, "Experimental Study of the Characteristics and Mechanism of Pool Boiling CHF Enhancement Using Nanofluids," Heat Mass Transfer, **45**(7), pp. 991–998.
[19] Şeşen, M., Khudhayer, W., Karabacak, T., and Koşar, A., 2010, "Compact Nanostructure Integrated Pool Boiler for Microscale Cooling Applications," Micro Nano Lett., **5**(4), pp. 203–206.
[20] Kim, I. T., Jeong, H. Y., and Chang, H. S., 2010, "An Experimental Study on CHF Enhancement in Flow Boiling Using Al_2O_3 Nano-Fluid," Int. J. Heat Mass Transfer, **53**(5-6), pp. 1015–1022.
[21] Park, D. S., Lee, W. S., Kang, S., Bang, C. I., Kim, H. J., Shin, S. H., Lee, W. D., and Lee, W. D., 2010, "Effects of Nanofluids Containing Graphene/Graphene-Oxide Nanosheets on Critical Heat Flux," Appl. Phys. Lett., **97**(2), p. 023103.
[22] Forrest, E., Williamson, E., Buongiorno, J., Hu, W. L., Rubner, M., and Cohen, R., 2010, "Augmentation of Nucleate Boiling Heat Transfer and Critical Heat Flux Using Nanoparticle Thin-Film Coatings," Int. J. Heat Mass Transfer, **53**(1-3), pp. 58–67.
[23] Morshed, A. M., Fanghao, Y., Yakut, M. A., Khan, J. A., and Li, C., 2012, "Enhanced Flow Boiling in a Microtube With Integration of Nano Wires," Appl. Therm. Eng., **32**, pp. 68–75.
[24] Phan, H. T., Caney, N., Marty, P., Colasson, S., and Gavillet, J., 2012, "Flow Boiling of Water on Nanocoated Surfaces in a Microchannel," ASME J. Heat Transfer, **134**, p. 020901.
[25] Ahn, H. S., Kang, S. H., Lee, C., Kim, J., and Kim, M. H., 2012, "The Effect of Liquid Spreading Due to Micro-Structures of Flow Boiling Critical Heat Flux," Int. J. Multiphase Flow, **43**, pp. 1–12.
[26] Betz, R. A., Jenkins, J., Kim, C., and Attinger, D., 2013, "Boiling Heat Transfer on Superhydrophilic, Superhydrophobic, and Superbiphilic Surfaces," Int. J. Heat Mass Transfer, **57**(2), pp. 733–741.
[27] Saeidi, D., and Alemrajabi, A. A., 2013, "Experimental Investigation of Pool Boiling Heat Transfer and Critical Heat Flux of Nanostructured Surfaces," Int. J. Heat Mass Transfer, **60**, pp. 430–449.
[28] Tang, Y., Tang, B., Li, Q., Qing, J., Lu, L., and Chen, K., 2013, "Pool-Boiling Enhancement by Novel Metallic Nanoporous Surface," Exp. Therm. Fluid Sci., **44**, pp. 194–198.
[29] Yongwei, C., Mingyan, L., and Longfei, H., 2013, "CaCO3 Fouling on Microscale-Nanoscale Hydrophobic Titania-Fluoroalkylsilane Films in Pool Boiling," AIChE J., **59**(7), pp. 2662–2678.
[30] Tenhaeff, W. E., and Gleason, K. K., 2008, "Initiated and Oxidative Chemical Vapor Deposition of Polymeric Thin Films: iCVD and oCVD," Adv. Funct. Mater., **18**(7), pp. 979–992.
[31] Lau, K. K., and Gleason, K. K., 2006, "Initiated Chemical Vapor Deposition (iCVD) of Poly (Alkyl Acrylates): An Experimental Study," Int. J. Sci., **39**(10), pp. 3695–3703.
[32] Chan, K., and Gleason, K. K., 2005, "Initiated Chemical Vapor Deposition of Linear and Cross-Linked Poly (2-Hydroxyethyl Methacrylate) for Use as Thin-Film Hydrogels," Langmuir, **21**(19), pp. 8930–8939.
[33] Alf, M. E., Asatekin, A., Barr, M. C., Baxamusa, S. H., Chelawat, H., Ozaydin-Ince, G., Petruczok, C. D., Sreenivasan, R., Tenhaeff, W. E., Trujillo, N. J., Vaddiraju, S., Xu, J., and Gleason, K. K., 2009, "Chemical Vapor Deposition of Conformal, Functional, and Responsive Polymer Films," Adv. Mater., **22**(18), pp. 1993–2027.
[34] Trujillo, N. J., Baxamusa, S. H., and Gleason, K. K., 2009, "Grafted Functional Polymer Nanostructures Patterned Bottom-Up by Colloidal Lithography and Initiated Chemical Vapor Deposition (iCVD)," Chem. Mater., **21**, pp. 742–750.
[35] Özdemir, M. R., and Koşar, A., 2013, "Thermally Developing Single-Phase Flows in Microtubes," ASME J. Heat Transfer, **135**(7), p. 074502.
[36] Özdemir, M. R., Kaya, A., and Koşar, A., 2011, "Low Mass Quality Flow Boiling in Microtubes at High Mass Fluxes," ASME J. Therm. Sci. Eng. Appl., **3**(4), p. 041001.
[37] Harvey, S. D., Vucelick, M. E., Lee, N. R., and Wright, B. W., 2002, "Blind Field Test Evaluation of Raman Spectroscopy as a Forensic Tool," Forensic Sci. Int., **125**(1), pp. 12–21.
[38] Constantini, A., Luciani, G., Annunziata, G., Silvestri, B., and Branda, F., 2006, "Swelling Properties and Bioactivity of Silica Gel/pHEMA Nanocomposites," J. Mater. Sci.: Mater. Med., **17**(4), pp. 319–325.
[39] Ozaydin-Ince, G., Demirel, G., Gleason, K. K., and Demirel, M. C., 2010, "Highly Swellable Free-Standing Hydrogel Nanotube Forests Soft Matter," Soft Matter, **6**, pp. 1635–1639.
[40] Colthup, N. B., Daly, L. H., and Wiberley, S, E., 1990, *Introduction to Infrared and Raman Spectroscopy*, Academic Press, New York, pp. 20–24.
[41] Kline, S., and McClintock, F, A., 1953, "Describing Uncertainties in Single-Sample Experiments," ASME Mech. Eng., **75**, pp. 3–8.
[42] Çengel, Y. A., and Cimbala, J. M., 2010, *Fluid Mechanics Fundamentals and Applications*, McGraw-Hill, New York.
[43] Özdemir, M. R., and Koşar, A., 2010, "Experimental Study on Single-Phase Flow in Microtubes at High Mass Flow Rates," ASME 2010 3rd Joint US-European Fluids Engineering Summer Meeting and 8th Intl' Conference on Nanochannels, Microchannels, and Minichannels, Montreal, Canada, Paper No. FEDS-ICNMM2010-30792.
[44] Kurtoğlu, M., Kaya., A., Gozuacik, D., Yagci-Acar, H. F., and Koşar, A., 2014, "Experimental Study on Convective Heat Transfer Performance of Iron Oxide Based Ferrofluids in Microtubes," ASME J. Therm. Sci. Eng. Appl., **6**, p. 034501.
[45] Tarasova, N. V., Leontiev, A., Hlopushin, V. I., and Orlov, V. M., 1966, "Pressure Drop of Subcooled Water and Steam-Water Mixture Flowing in Heated Channels," Proceedings of 3rd International Heat Transfer Conference, Paper No. 113.
[46] Dormer, J., and Bergles, A. E., 1964, "Pressure Drop With Surface Boiling in Small Diameter Tubes," Department of Mechanical Engineering, MIT, Report No. 8767-31.
[47] Morini, G. L., 2006, "Scaling Effects for Liquid Flows in Microchannels," Heat Transfer Eng., **27**, pp. 64–73.

[48] Kroeker, C. J., Soliman, H. M., and Ormiston, S. J., 2004, "Three Dimensional Thermal Analysis of Heat Sinks With Circular Cooling Micro-Channels," Int. J. Heat Mass Transfer, **47**, pp. 4733–4744.
[49] Zhai, L., Cebeci, F. Ç., Cohen, R. E., and Rubner, M. F., 2004, "Stable Superhydrophobic Coatings From Polyelectrolyte Multilayers," Nano Lett., **4**(7), pp. 1349–1353.
[50] Lenz, P., and Lipowsky, R., 1998, "Morphological Transitions of Wetting Layers on Structured Surfaces," Phys. Rev. Lett., **80**(9), pp. 1920–1923.
[51] Ji, S., Liu, C., Son, J. G., Gotrik, K., Craig, G. S. W., Gopalan, P., Himpsel, F. J., Char, K., and Nealey, P. F., 2008, "Generalization of the Use of Random Copolymers to Control the Wetting Behavior of Block Copolymer Films," Macromolecules, **41**(23), pp. 9098–9103.
[52] Webb, R. L., 1994, *Principles of Enhanced Heat Transfer*, John Wiley and Sons, New York, Chap. 11.
[53] Yabe, A., Mori, Y., and Hijikata, K., 1995, "Active Heat Transfer Enhancement by Utilizing Electric Fields," Annu. Rev. Heat Transfer, **7**, pp. 193–244.
[54] Yabe, A., Taketani, T., Maki, H., Takahashi, K., and Nakadai, Y., 1992, "Experimental Study of Electro-Hydrodynamically (EHD) Enhanced Evaporator for Nonazeotropic Mixtures," ASHRAE Trans., **98**, pp. 455–460.
[55] Kandlikar, S. G., 2010, "A Scale Analysis Based Theoretical Force Balance Model for Critical Heat Flux (CHF) During Saturated Flow Boiling in Microchannels and Minichannels," ASME J. Heat Transfer, **132**(8), p. 081501.
[56] Mudawar, I., and Bowers, M. B., 1999, "Ultra-High Critical Heat Flux (CHF) for Subcooled Water Flow Boiling: CHF Data and Parametric Effects for Small Diameter Tubes," Int. J. Heat Mass Transfer, **42**, pp. 1405–1428.
[57] Kuo, J. C., Kosar, A., Peles, Y., Virost, S., Mishra, C., and Jensen, M. K., 2006, "Bubble Dynamics During Boiling in Enhanced Surface Microtubes," J. Microelectromech. Syst., **15**(6), pp. 1514–1527.
[58] Bergles, A. E., 1963, "Subcooled Burnout in Tubes of Small Diameter," ASME Paper No. 63-WA-182.
[59] Groeneveld, D. C., 1996, "The 1995 Look-Up Table for Critical Heat Flux in Tubes," Appl. Therm. Eng., **163**, pp. 1–23.
[60] Celata, G. P., 1993, "Recent Achievements in the Thermal Hydraulics of High Heat Flux Components in Fusion Reactors," Exp. Therm. Fluid Sci., **7**(4), pp. 263–278.
[61] Vandervort, C. L., Bergles, A. E., and Jensen, M. K., 1994, "An Experimental Study of Critical Heat Flux in Very High Heat Flux Subcooled Boiling," Int. J. Heat Mass Transfer, **37**(1), pp. 161–173.
[62] Hall, D. D., and Mudawar, I., 2000, "Critical Heat Flux (CHF) for Water Flow in Tubes—II: Subcooled CHF Correlations," Int. J. Heat Mass Transfer, **43**(14), pp. 2605–2640.
[63] Brutin. D., and Tadrist, L., 2004, "Pressure Drop and Heat Transfer Analysis of Flow Boiling in a Minichannel: Influence of the Inlet Condition on Two-Phase Flow Stability," Int. J. Heat Mass Transfer, **47**, pp. 2365–2377.
[64] Ali, Y. M., Yang, F., Fang, R., Chen, L., and Khan, J., 2011, "Thermohydraulic Characteristics of A Single-Phase Microtube Heat Sink Coated With Copper Nanowires," Front. Heat Mass Transfer, **2**, pp. 451–534.
[65] McHale, J. P., and Garimella, S., 2010, "Bubble Nucleation Characteristics in Pool Boiling of a Wetting Liquid on Smooth and Rough Surfaces," Int. J. Multiphase Flow, **36**, pp. 249–260.